Voltage-gated sodium channel activity mediates sea urchin larval skeletal patterning through spatial regulation of Wnt5 expression

Christopher F. Thomas[1,2], Dakota Y. Hawkins[1,3], Viktoriya Skidanova[1], Simone R. Marrujo[4], Janay Gibson[5], Ziqing Ye[6], Cynthia A. Bradham[1,2,3,*].

[1]Department of Biology, Boston University, Boston, MA 02215, USA. [2]Program in Cell and Molecular Biology, Boston University, Boston, MA 02215, USA. [3]Program in Bioinformatics, Boston University, Boston, MA 02215, USA. [4]Whitworth University, Spokane, WA 99251, USA. [5]Alabama A&M University, Huntsville, AL 35811, USA. [6]George School, Newtown, PA 18940, USA.

* address correspondence to cbradham@bu.edu

Running title: Ion channels & skeletal pattern

Key Words: PMCs, Biomineralization, pattern formation, skeleton, Wnt, sea urchin

Summary statement: Inhibition of voltage-gated sodium channels perturbs Wnt5-mediated patterning of the sea urchin larval skeleton.

Abstract

Defining pattern formation mechanisms during embryonic development is important for understanding the etiology of birth defects and to inform tissue engineering approaches. In this study, we used tricaine, a voltage-gated sodium channel (VGSC) inhibitor, to show that VGSC activity is required for normal skeletal patterning in *Lytechinus variegatus* sea urchin larvae. We demonstrate that tricaine-mediated patterning defects are rescued by an anesthetic-insensitive version of the VGSC LvScn5a. This channel is expressed in the posterior ventrolateral ectoderm where it spatially overlaps with Wnt5. We show that VGSC activity is required to spatially restrict Wnt5 expression to this ectodermal region that is adjacent and instructive to clusters of primary mesenchymal cells (PMCs) where secretion of the larval skeleton is initiated as triradiates. Tricaine-mediated Wnt5 spatial expansion correlates with the formation of ectopic PMC clusters and triradiates. These tricaine-mediated defects are rescued by Wnt5 knock down, indicating that the spatial expansion Wnt5 is responsible for the patterning defects induced by VGSC inhibition. These results demonstrate a novel connection between bioelectrical status and the spatial control of patterning cue expression during embryonic pattern formation.
(180 words)

Introduction

The action of ion channels, pumps and transporters is responsible for regulating processes such as wound healing, regeneration, and development of organisms such as insects, vertebrates, and echinoderms (Akasaka et al., 1997; Cole and Woodruff, 2000; Nuccitelli, 2003; Kawakami et al., 2005; Adams et al., 2006; Adams et al., 2007; Levin, 2012; Shipp and Hamdoun, 2012; Stumpp et al., 2012; Beane et al., 2013; Levin, 2014; Schatzberg et al., 2015; Hu et al., 2018). During sea urchin development, ion channels mediate both the fast and slow blocks to polyspermy and play a role in regulating left-right symmetry breaking, ventral specification, skeletal patterning, and PMC biomineralization (Jaffe, 1976; Hibino et al., 2006; Bergeron et al., 2011; Schatzberg et al., 2015; Piacentino et al., 2016b). To uncover additional roles for ion channels in sea urchin development, we performed a screen of ion channel inhibitors. This screen revealed that inhibition of voltage-gated sodium channels (VGSCs) by tricaine elicits patterning defects in the larval skeleton. Tricaine is a local anesthetic commonly used for sedation of aquatic organisms and is a potent inhibitor of VGSCs (Schoettger, 1967; Frazier and Narahashi, 1975; Letcher, 1992; Cakir and Strauch, 2005; Attili and Hughes, 2014).

The sea urchin larval skeleton is secreted by the primary mesenchyme cells (PMCs) (Lyons et al., 2012). Prior to gastrulation, the PMCs undergo an epithelial-to-mesenchymal transition (EMT) and ingress into the blastocoel. At late gastrula stage, the PMCs have migrated into a stereotypical spatial pattern comprised of a posterior ring of cells around the hindgut with bilateral ventrolateral clusters of cells; cords of cells extend from the clusters towards the anterior territory. This cellular "ring-and-cords" organization is considered the primary (1°) skeletal pattern. Calcium from the surrounding sea water is precipitated as $CaCO_3$ within PMC vesicles in a process that requires the proton-potassium ATPase (HKA) and the SLC4a10 bicarbonate transporter (Vidavsky et al., 2014; Schatzberg et al., 2015; Hu et al., 2018); this process is initiated in the ventrolateral PMC clusters to produce bilateral skeletal triradiates; the radii are then extended as spicules along the 1° pattern. Subsequent PMC migration from the ring-and-cords pattern produces the secondary (2°) pattern that yields the long skeletal elements (Ettensohn and Malinda, 1993; Piacentino et al., 2015; Piacentino et al., 2016a; Piacentino et al., 2016b).

In 1937, von Ubisch suggested that cues from the adjacent ectoderm are responsible for coordinating the migration of the PMCs within the blastocoel (von Ubisch, 1937). Transplantation experiments have been key in confirming that the migratory behavior of the PMCs is controlled by cues received from the ectoderm. For example, treating embryos with $NiCl_2$ results in skeletal patterning defects (Hardin et al., 1992). Later work showed that transplanting control PMCs into $NiCl_2$-treated PMC-less hosts phenocopied those skeletal patterning defects whereas the reciprocal experiment resulted in control-like skeletons, indicating that the nickel-mediated skeletal patterning defect was specific to the ectoderm (Armstrong et al., 1993). Subsequent studies uncovered the identity of specific ectodermal skeletal patterning cues such as vascular endothelial growth factor (VEGF) (Duloquin et al., 2007). VEGF is initially expressed in two ventrolateral patches in the ectoderm, while the expression of its receptor VEGFR is enriched in the adjacent PMC clusters (Duloquin et al., 2007; Adomako-Ankomah and Ettensohn, 2013). Wnt5 is another ventrolateral ectodermal patterning cue that is required for biomineralization and is sufficient to induce abnormal PMC migration and ectopic skeletogenesis (McIntyre et

al., 2013). Our group has uncovered many other ectodermal patterning cues, including the sulfate transporter SLC26a2/7, Univin and its receptor Alk4/5/7, and BMP5-8 (Piacentino et al., 2015; Piacentino et al., 2016a; Piacentino et al., 2016b). However, the roles that ion channels and pumps play in regulating skeletal patterning remain incompletely understood.

VGSCs are classically known to induce action potentials in excitable cells such as neurons, and knockout experiments in mice show that VGSCs are required for normal development of the central nervous system (CNS) (Harris and Pollard, 1986; Planells-Cases et al., 2000; Yu et al., 2006). In zebrafish, expression of the VGSC isoform $Na_v1.5$ is required for normal heart development (Chopra et al., 2010). VGSCs have also been identified in other cell types including fibroblasts, glia, immune cells, and cancer cells where their functions remain less clear (Brackenbury et al., 2008).

In this study, we show that inhibition of VGSC activity in *Lytechinus variegatus* (Lv) embryos elicits skeletal patterning defects and that these defects can be rescued via overexpression of an anesthetic insensitive version of the VGSC Scn5a. We show that VGSC activity is required during gastrulation for normal skeletal patterning and for normal spatial positioning of PMCs. We find that VGSC inhibition results in spatial expansion of Wnt5 in the ventrolateral ectoderm, the presence of ectopic PMC clusters that express Jun, and the occurrence of supernumerary skeletal triradiates. Finally, we show that hallmark tricaine-mediated skeletal patterning defects are rescued by partial knockdown of Wnt5. Together, these results establish a crucial role for VGSC activity in the spatial restriction of Wnt5 in the ventrolateral ectoderm that is required for normal skeletal patterning.

Results

VGSC activity is required for normal skeletal patterning during gastrulation

We performed a pharmacological screen of ion channel inhibitors and discovered that tricaine, an inhibitor of voltage-gated sodium channels (VGSCs), elicits skeletal patterning defects (Fig. 1A-B). We scored the defects using our established in-house rubric (Piacentino et al., 2016b) and identified specific skeletal patterning abnormalities, including loss of skeletal rods, the presence of ectopic skeletal rods, and orientation defects (Fig. 1B). The ventral transverse (VT) rods were the most frequently absent rods amongst tricaine-treated embryos, whereas the most commonly observed orientation defects were

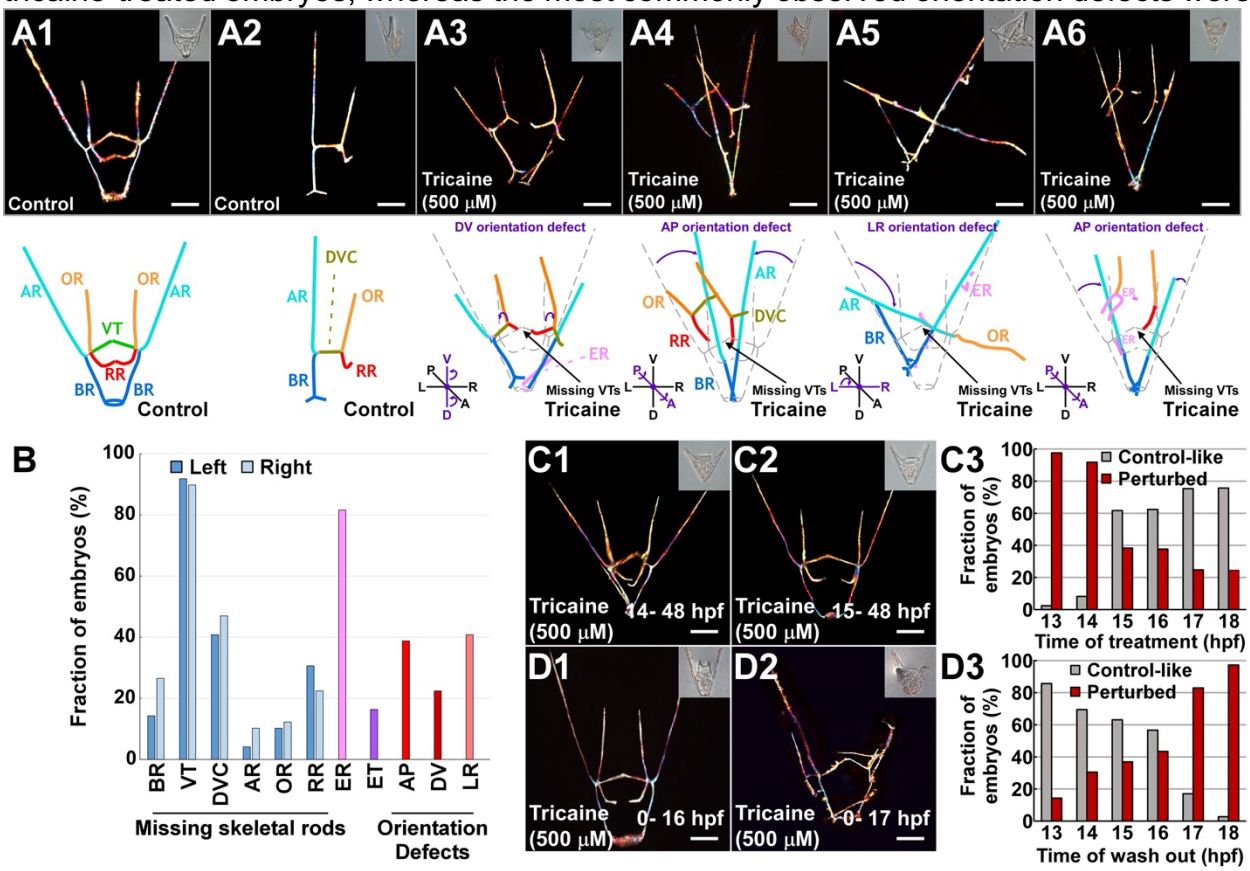

Figure 1. Voltage-gated sodium channel (VGSC) activity is required for normal skeletal patterning during gastrulation.
A. Representative skeletal birefringence images of control (A1-2, upper panels) and tricaine-treated (A3-6, upper panels) embryos are shown at 48 hpf with corresponding morphology images (DIC) inset. Schematized versions of each skeleton are shown (A lower panels) with skeletal elements indicated in color, including body rods (BRs, blue), aboral rods (ARs, cyan), ventral transverse rods (VTs, green), dorsal-ventral connecting rods (DVCs, dark yellow), recurrent rods (RRs, red), oral rods (ORs, orange). Ectopic rods (ERs, pink) are also indicated. Orientation defect exemplars show abnormal orientations about the AP, DV, or LR axes as indicated (A3-6). B. Skeletal defects including element losses, the presence of ectopic rods (ER), ectopic triradiates (ET), and orientation defects about each body axis are plotted as the percentage of embryos exhibiting each defect (n = 49). C-D. Embryos that were treated with tricaine during the indicated hours post-fertilization (hpf) (C1, C2, D1, D2), are shown at pluteus stage (48 hpf) as skeletal patterns (birefringence) with corresponding DIC images inset. Embryos were treated with tricaine at the indicated time points (C) or treated with tricaine then removed from the drug at the indicated time points (D), then scored for patterning defects at pluteus stage (C3, D3); n ≥ 247 per condition (C3); n ≥ 177 per condition (D3). See also Fig. S1. Scale bars are 50 μm for all figures unless otherwise indicated.

anterior-posterior and left-right orientation defects (Fig. 1B). We also observed a high frequency of ectopic rods and a lower but measurable frequency of ectopic triradiates (ETs) (Fig. 1B, ER). The occurrence of ectopic triradiates is notable in that this defect has not been previously detected with other skeletal patterning cue perturbations (Duloquin et al., 2007; Adomako-Ankomah and Ettensohn, 2013; McIntyre et al., 2013; Piacentino et al., 2015; Piacentino et al., 2016a; Piacentino et al., 2016b). To determine the temporal window during which VGSC activity is required for skeletal patterning, we performed timed treatment and washout experiments with tricaine, then assessed the resulting embryos for skeletal patterning defects at the pluteus stage (Fig. 1C-D, S1). We found that inhibiting VGSCs prior to 14 hpf results in a large proportion of embryos with patterning defects, while treatment after 14 hpf results in the majority of embryos developing control-like skeletons (Fig. 1C, S1B1-7, S1C). In the converse experiments, we found that inhibiting VGSCs from fertilization until 17 hpf results in the majority of embryos developing defective skeletons. However, removal of tricaine at 16 hpf or earlier results in normal skeletal patterns within the majority of larva (Fig. 1D, S1). We scored

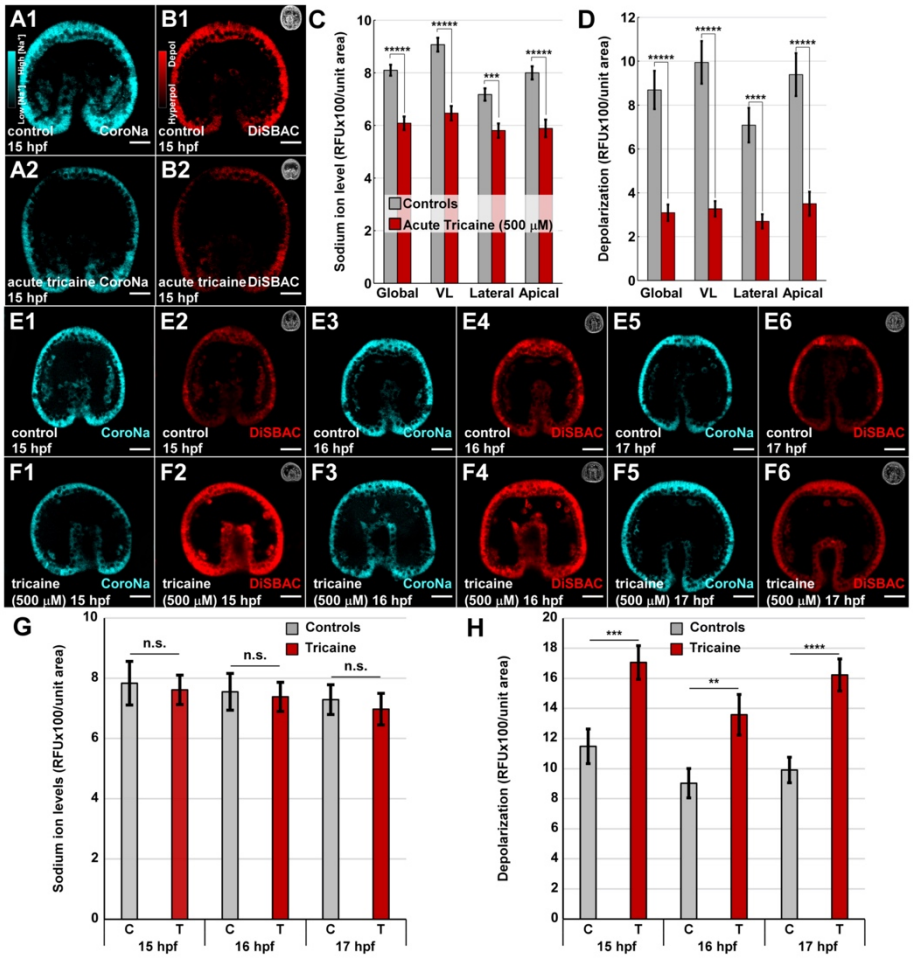

Figure 2. VGSC inhibition is sufficient to perturb intracellular sodium ion concentration and membrane voltage (V_{mem}).

A-D. Sodium ions were visualized with the fluorescent reporter CoroNa (cyan), and V_{mem} was visualized with DiSBAC (red) in the same live embryos; the signal ranges are shown using custom LUTs (inset in A1, B1). Control (A1, B1) and tricaine-treated (A2, B2) embryos were analyzed at 15 hpf immediately following tricaine treatment to determine tricaine's acute effects. Relative sodium ion levels (C) and V_{mem} (D) were quantified in the indicated ectodermal territories and are shown as the average RFU/area ± s.e.m.; n = 37 embryos per condition; *** $p < 10^{-3}$; ***** $p < 10^{-5}$ (student *t*-test). E-H. Sodium ions and V_{mem} were visualized in controls (E) and embryos treated with tricaine (F) from fertilization, then analyzed as in panels C-D. at the indicated time points during gastrulation. Relative signal levels were quantified as in panel C-D (G-H, see also Fig. S2); n ≥ 24 per condition; ** $p < 10^{-2}$; *** $p < 10^{-3}$; **** $p < 10^{-4}$ (student *t*-test). Scale bars represent 20 μm.

the patterning defects in embryos exposed to tricaine for defined temporal intervals and found that primary skeletal defects exhibited a saddle-like profile, dominating the earliest and latest intervals but not between, while orientation and secondary defects were most evident in the latest intervals (Fig. S1D-E). Taken together, these data show that tricaine-sensitive VGSC activity is required during gastrulation from 14 to 17 hpf for normal skeletal patterning.

VGSC inhibition is sufficient to perturb both intracellular sodium ion concentration and transmembrane voltage

To functionally confirm that tricaine inhibits VGSCs in sea urchin embryos, we investigated the effect of tricaine treatment on transmembrane voltage (V_{mem}) and sodium ion levels by using the fluorescent reporters DiSBAC and CoroNa-AM, respectively (Epps et al., 1994; Meier et al., 2006; Adams and Levin, 2012; Rodriguez-Sastre et al., 2019). Since VGSC activity is required for skeletal patterning from 14 to 17 hpf, we asked how tricaine treatment affects V_{mem} and sodium ion levels during this developmental window. To unambiguously define the effects of tricaine treatment, we first subjected the embryos to tricaine treatment only minutes prior to measuring V_{mem} and sodium levels to determine the acute response to the inhibitor. We found that acute VGSC inhibition results in reduced sodium ion levels relative to controls, consistent with expectations (Fig. 2A1-2). Quantification of the signal shows that relative to controls, sodium ion levels were significantly decreased in tricaine-treated embryos globally and in each of the ectodermal regions measured, including posterior ventrolateral tissue adjacent to the PMC clusters, the apical territory, and the anterior lateral ectodermal region between those two territories (Fig. 2C). When we similarly measured V_{mem} in the ectoderm, we found that tricaine-treated embryos are significantly hyperpolarized relative to controls (Fig. 2B1,2) globally as well as in each measured ectodermal region (Fig. 2D), as expected upon inhibition of VGSCs. These data show that tricaine functionally inhibits VGSC activity in sea urchin embryos.

To observe the effects of long-term VGSC inhibition, we treated embryos with tricaine from fertilization to either mid- or late gastrula stage, then measured V_{mem} and sodium ion levels. In this case, we found that long-term tricaine treatment does not result in a significant decrease to sodium ion levels relative to controls in any of the ectodermal regions measured (Fig. 2E, G, S2A). Surprisingly, long-term VGSC inhibition resulted in significant depolarization of embryos relative to controls at 15, 16, and 17 hpf (Fig. 2F, H, S2B), in contrast to the acute effects of tricaine. This observed depolarization was unexpected since VGSC inhibition would be expected to hyperpolarize cells due to the block to sodium ion influx. The observed depolarization along with the absence of decreased sodium ion levels after prolonged tricaine treatment suggests that compensatory processes restore normal sodium ion levels, possibly at the expense of V_{mem}, via movement of ions, including sodium ions, through other channels. These data show that long-term tricaine treatment is sufficient to significantly depolarize ectodermal V_{mem} in the developmental stages during which VGSC activity is required for normal skeletal patterning.

Expression of a drug-resistant VGSC is sufficient to rescue tricaine-mediated skeletal patterning defects

VGSCs are integral membrane proteins made up of a pore-forming α subunit with associated auxiliary β subunits that enable the influx of sodium ions into cells in response to membrane depolarization (Ragsdale et al., 1994; Catterall, 2000, 2014). LvScn5a is the sole annotated VGSC within the developmental transcriptome for Lv (Hogan et al., 2020). LvScn5a expression is elevated during gastrulation when embryos are sensitive to tricaine, then becomes highly elevated after gastrulation, likely corresponding to neural development (Hogan et al., 2020) and coinciding with skeletal development, especially for secondary skeletal components (Fig. 3A). Spatial expression analysis shows that

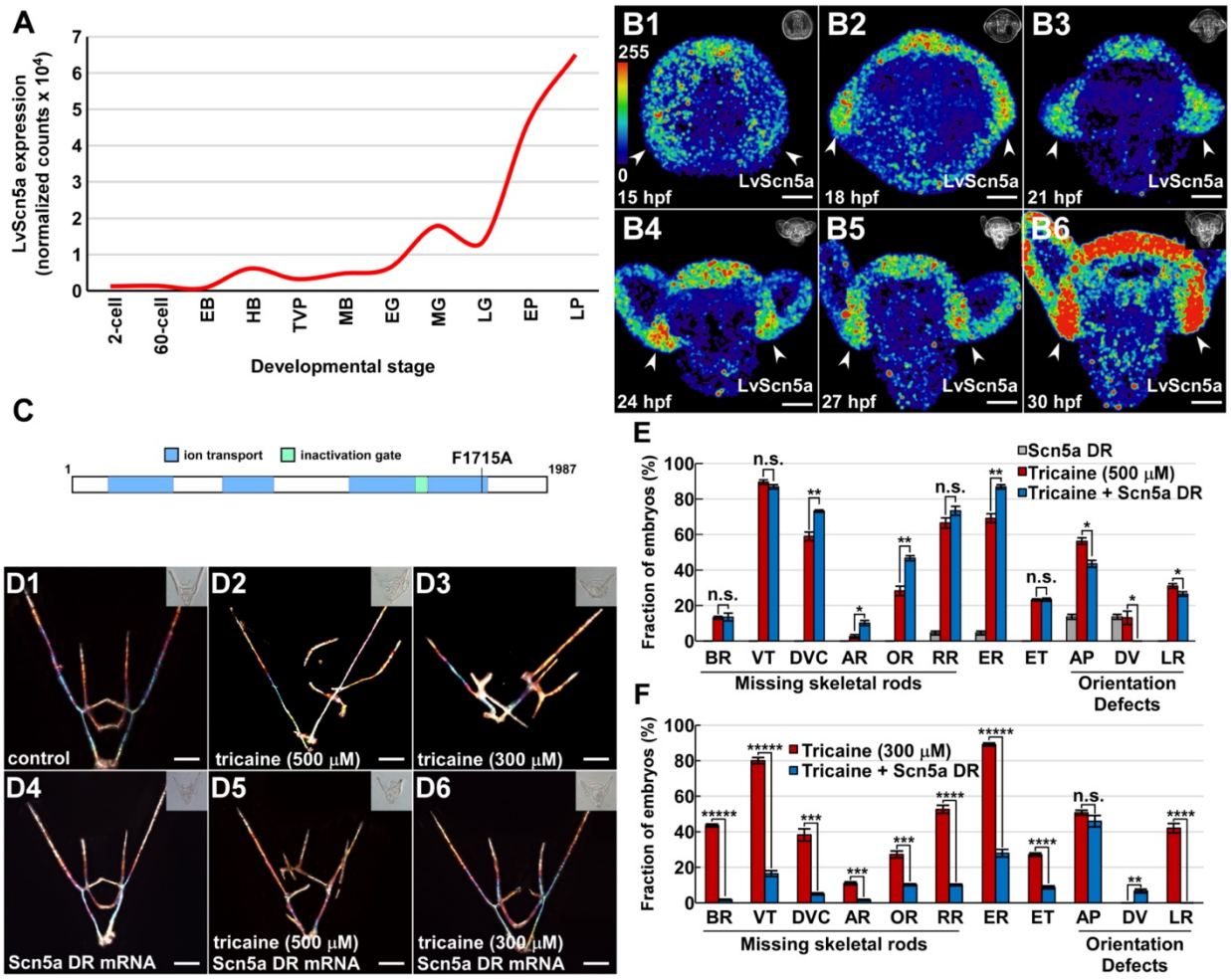

Figure 3. Tricaine-mediated skeletal patterning defects are rescued by overexpression of drug-resistant (DR) LvScn5a.

A. The temporal expression of LvScn5a is shown at the indicated stages as normalized counts (from Hogan, et al., 2020). B. Control embryos were fixed at the indicated developmental timepoints, then subjected to FISH for LvScn5a. Z-projected embryos are shown pseudocolored using a custom LUT (inset in B1). C. The schematic shows the LvScn5A gene, with ion transport domains and the DR mutation indicated. The schematic is drawn to scale. D. Control zygotes (D1-3) or zygotes injected with LvScn5a DR mRNA (D4-6) were either untreated (D1, 4) or treated with tricaine at 500 μM tricaine (D2, 5), or 300 μM (D3, 6), and are shown at the pluteus stage as in Fig. 1A. The frequency of the indicated skeletal patterning defects is shown as the average percentage of embryos with each defect ± s.e.m., with tricaine at 500 (E) or 300 (F) μM; see Fig. 1 for element names and abbreviations; n ≥ 30 per condition; * $p < 0.05$; ** $p < 10^{-5}$; *** $p < 10^{-10}$; **** $p < 10^{-20}$; ***** $p < 10^{-40}$; n.s. not significant (weighted *t*-test).

LvScn5a is expressed in the ventrolateral and apical ectoderm at mid and late gastrula stages (Fig. 3B), during the interval of sensitivity to tricaine (Fig. 1C-D). Between 18 and 27 hpf, the expression domain of LvScn5a expands to connect the VL and apical expression domains (Fig. 3B), appearing to correspond spatially with the ciliary band (see Fig. S4C). Since the ciliary band includes neurons, this expression pattern in older embryos and larvae fits with expectations.

Tricaine is a local anesthetic (LA) that reversibly inhibits VGSCs by binding to anesthetic binding sites within the protein (Ragsdale et al., 1994; Cakir and Strauch, 2005; Ramlochansingh et al., 2014). The LA binding domain in the pore of the VGSC was identified through site directed mutagenesis using iterative alanine substitutions for each residue, then testing sodium ion conductance (Ragsdale et al., 1994); in this way, the LA-insensitive F1760A mutant was identified. The F1760A substitution eliminates a critical binding domain for LAs, which significantly attenuates channel inhibition by LAs including tricaine (Ragsdale et al., 1994; Wright et al., 1998; Nau et al., 2000; Nau and Wang, 2004; Carboni et al., 2005; Pless et al., 2011; Stoetzer et al., 2016).

We next asked whether overexpression of an anesthetic-insensitive version of LvScn5a could rescue the skeletal patterning defects induced by tricaine treatment. We produced a drug-resistant (DR) version of LvScn5a by introducing the heterologous point mutation F1715A in domain IV of LvScn5a that corresponds to the F1760A mutation in human Scn5a (Fig. 3C). Embryos that were microinjected with LvScn5a DR mRNA displayed very few skeletal patterning defects, the most prevalent of which was an AP orientation defect in a small fraction of embryos (Fig. 3D4, E). Controls treated with 500 μM tricaine exhibited the typical tricaine-induced skeletal patterning defects (Fig 3D2). The combination of DR Scn5a and tricaine resulted in skeletons that more closely approach normal patterns (Fig. 3D5); however, DR Scn5a-expressing embryos failed to exhibit a significant rescue of tricaine-induced skeletal patterning defects (Fig. 3E). The improved appearance of some tricaine-treated embryos that express DR Scn5a compared to tricaine-treated controls prompted us to repeat this rescue experiment with a lower dose of tricaine. We originally selected 500 μM as the operating dose for tricaine since the penetrance of the phenotype was nearly 100% at that dose (Fig. S3). For these experiments, we tested 300 μM, which produces the same phenotype as 500 μM, but with only 80% penetrance (Fig. S3). Controls treated with 300 μM tricaine exhibited the hallmark skeletal patterning defects associated with tricaine treatment, including loss of VTs, LR orientation defects, and the appearance of ectopic skeletal rods (Fig. 3D3, F). Embryos injected with LvScn5a DR mRNA and treated with 300 μM tricaine exhibited a dramatic and significant recovery of skeletal patterning defects, including a rescue of VTs, reduction in the frequency of ectopic rods, and no incidences of LR orientation defects (Fig. 3D6, F). The finding that LvScn5a DR mRNA is sufficient to rescue the majority of the tricaine-induced skeletal patterning defects in embryos treated with 300 μM tricaine indicates that, aside from abnormal AP orientations, the tricaine-mediated defects are due to the specific inhibition of Scn5a. Interestingly, AP orientation defects were not rescued, suggesting that tricaine treatment elicits this skeletal patterning defect via a mechanism other than inhibition of VGSCs. The failure of LvScn5a DR mRNA to significantly rescue skeletal patterning at a higher tricaine dose suggests that the mutation introduced in the DR LvScn5a gene is insufficient to completely prevent the binding of tricaine at that dose. Therefore, at high enough tricaine concentrations, a sufficient amount of tricaine is able

to bind to the exogenously expressed LvScn5a channel, resulting in its inhibition with phenotypic consequences.

VGSC activity is not required for DV axis specification or neuronal differentiation

The observation that VGSC inhibition elicits skeletal patterning defects prompted us to assess the effects of tricaine exposure on the ectoderm. We first assessed neuronal differentiation by visualizing serotonin- and synaptotagmin B (synB)-positive neurons (Bradham et al., 2009; Yaguchi et al., 2010). Control embryos possessed both sets of neurons in normal spatial patterns (Fig. S4A). In tricaine-treated embryos, the number of serotonergic neurons appears normal. The shortened arms of tricaine-treated embryos result in crowding of the synB neurons; however, their number and spatial arrangement appears normal in the context of that abnormal morphology (Fig. S4B). Thus, tricaine does not affect neural specification or patterning at 48 hpf. We also assessed the ciliary band (CB), which is a narrow ectodermal region that is spatially restricted to the boundary between the dorsal and ventral territories of the embryo (Yaguchi et al., 2010). Since the CB fate is repressed by DV specifying TGFβ signals, it is a useful readout for DV perturbations (Duboc et al., 2004; Bradham et al., 2009; Yaguchi et al., 2010). We used immunostaining to show that the CB is restricted to a normal, narrow band in both control and tricaine-treated embryos (Fig. S4C-D), indicating that tricaine treatment does not perturb DV specification. To corroborate that result, we performed single molecule (sm) FISH for LvChordin and LvIrxA, markers of ventral and dorsal, respectively. The spatial expression of each gene was not significantly affected by tricaine treatment relative to controls, nor was the inferred size of the CB between them (Fig. S4E-K), indicating that VGSC activity is not required for ectodermal DV specification.

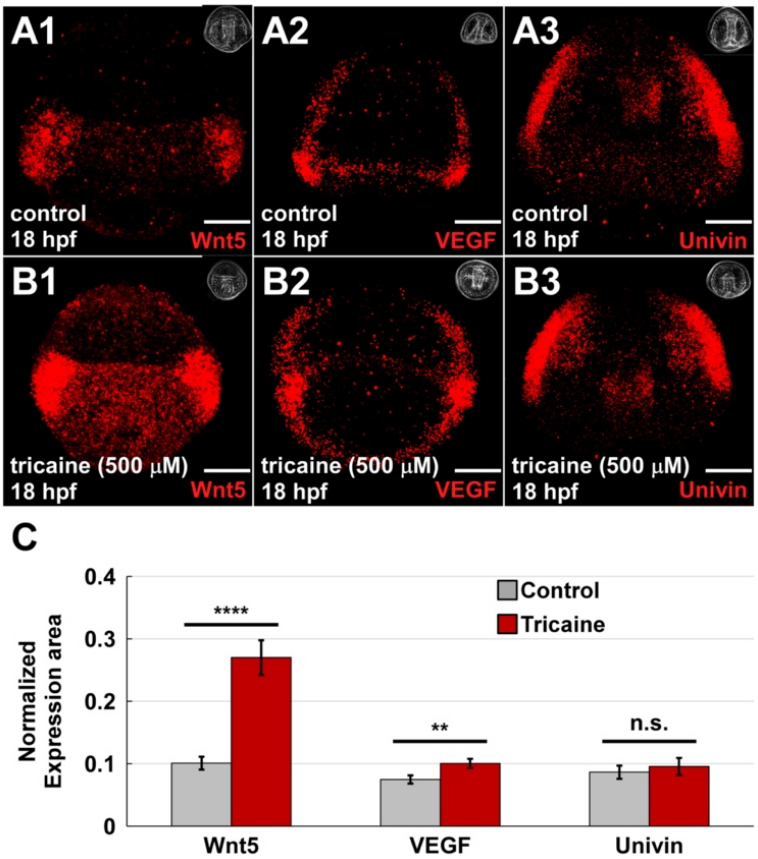

Figure 4. VGSC activity is required to spatially restrict the gene expression domains of Wnt5 and VEGF but not Univin.
A-B. Control (A) and tricaine-treated (B1) late gastrula-stage embryos were subjected to HCR FISH for the ectodermal patterning genes Wnt5 (1), VEGF (2), or Univin (3). C. The normalized area of the expression domains for each gene is shown as the average ± s.e.m.; n ≥ 30 (Wnt5, VEGF) or n ≥ 17 (Univin); ** $p < 10^{-2}$; ****; $p < 10^{-6}$; n.s., not significant (student *t*-test). Scale bars represents 20 μm. See also Fig. S4.

Skeletal patterning cues in the ventrolateral ectoderm are perturbed in tricaine-treated embryos

The posterior ventrolateral (VL) ectoderm corresponds with the expression domain for two ectodermal skeletal cues, LvWnt5 and LvVEGF, and is posterior to the expression of a third cue, Univin (Duloquin et al., 2007; Adomako-Ankomah and Ettensohn, 2013; McIntyre et al., 2013; Piacentino et al., 2015; Piacentino et al., 2016b). To test whether VGSC inhibition impacts the expression of these genes, we next performed smFISH for each cue in control and tricaine-treated embryos (Fig. 4A-B). We found that both LvWnt5 and LvVEGF, but not LvUnivin, are significantly spatially expanded in tricaine-treated embryos relative to controls, with the most dramatic effect on Wnt5 (Fig. 4C). Thus, VGSC inhibition is sufficient to spatially expand the expression domains of Wnt5, and to a lesser extent, VEGF, but is insufficient to affect the expression of the spatially adjacent cue Univin.

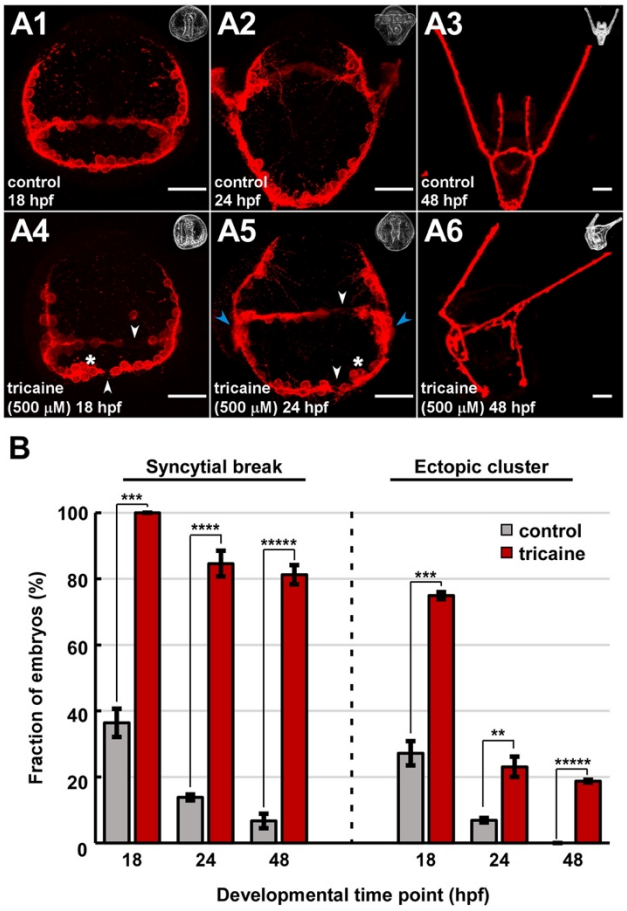

Figure 5. VGSC activity is required for normal PMC migration and syncytial integrity.
A. PMCs were immunolabeled in control (1-3) and tricaine-treated (4-6) embryos at the indicated timepoints and are shown as confocal z-projections; the corresponding phase contrast images are inset. Defects include syncytial breaks (white arrowheads), ectopic clusters (white asterisks), and lack of normal migration into the secondary pattern (blue arrowheads). B. The fraction of embryos exhibiting each defect is shown as the average percentage ± s.e.m.; n ≥ 19 for control and tricaine at 18 and 24 hpf; n ≥ 15 for control and tricaine at 48 hpf; * $p < 0.05$; ** $p < 10^{-4}$; *** $p < 10^{-8}$; **** $p < 10^{-12}$; ***** $p < 10^{-16}$; n.s. not significant (weighted *t*-test). See also Fig. S5. Scale bars in A1,2, 4, and 5 represents 20 μm; the remainder are 50 μm.

VGSC activity is required for normal PMC migration and syncytial integrity

The observation that VGSC inhibition elicits skeletal patterning defects and perturbs the spatial expression of the ectodermal patterning genes VEGF and Wnt5 led us to next evaluate the effects of tricaine on the skeletogenic PMCs. In late gastrula-stage controls, the PMCs are arranged in the ring-and-cords pattern with ventrolateral clusters in which skeletogenesis initiates; the PMCs are connected by a syncytial cable in which the biomineral is deposited (Fig. 5A1). In tricaine-treated late gastrula-stage embryos, the PMCs approximate the ring-and-cords pattern; however, there are a number of anomalies (Fig. 5A4), including breaks in the syncytial cable, "rogue" PMCs that failed to incorporate into the syncytium, and ectopic PMC clusters. We quantified the frequency of breaks and ectopic clusters, and found that, at late gastrula stage,

100% of the tricaine-treated embryos exhibited a syncytial break and 75% exhibited at least one ectopic cluster (Fig. 5B). Syncytial breaks were most common in the ventral part of the ring and least common in the cords at late gastrula stage (18 hpf) and were fewer thereafter (Fig. S5A), implying that tricaine-treated embryos on average were able to resolve some of the PMC anomalies after late gastrula stage. Rogue PMCs were present in controls, and were significantly increased among tricaine-treated embryos at each of the time points that were assessed (Fig. S5A)

In 24 hpf control embryos (late prism stage, Fig. 5A2), the PMCs have begun migrating from the initial, primary PMC pattern to form the secondary elements. However, in tricaine-treated 24 hpf embryos, the PMCs have failed to begin secondary migration and appear stalled in the late gastrula-stage pattern (Fig. 5A5). In late pluteus-stage (48 hpf) controls, the PMCs occupy normal primary and secondary positions (Fig. 5A3), while in tricaine-treated late plutei, the PMCs have migrated to some but not all of the normal secondary positions; abnormal PMC positioning that corresponds with skeletal patterning defects is evident (Fig. 5A6). PMC features in addition to migration defects are abnormal in tricaine-treated embryos relative to controls: syncytial breaks persist in late plutei although at fewer per embryos with time, while the number of embryos with ectopic clusters is reduced from 75 to 19% compared to controls with time (Fig. 5B, S5B). The large reduction in ectopic clusters after late gastrula stage might reflect the normal migration of PMCs from the clusters (including ectopic clusters), diminishing them, during secondary skeletal patterning. Consistent with that possibility, we observed extra triradiates in some tricaine-treated embryos that probably reflect these prior ectopic PMC clusters; the ectopic skeletal rods induced by tricaine might also reflect partial development of ectopic triradiates (Fig. 1B). Finally, the number of embryos with rogue PMCs is variable; however, there is a significant increase in the incidence of tricaine-treated embryos with rogue PMCs compared to controls (Fig. S5A). The number of rogue PMCs per embryo is also significantly increased at each time point, but most dramatically at 48 hpf, in tricaine-treated embryos (Fig. S5B). We also note a surprising reduction in rogue PMCs in each condition at 24 hpf, suggesting that this population undergoes dynamic changes rather than remaining a static population that remains disconnected from the PMC syncytium. Taken together, these data show that VGSC activity is required for timely PMC migration, normal spatial positioning of PMCs, continuity of the PMC syncytium, prevention of rogue PMCs, and restriction to only two PMC clusters.

VGSC activity is required to spatially restrict expression of c-Jun and Pks2

Over the course of skeletal patterning, the PMCs diversify, reflected by subpopulations of PMCs that exhibit differential gene expression; this diversification likely occurs in response to the receipt of patterning cues (Croce et al., 2003; Gross et al., 2003; Sun and Ettensohn, 2014; Piacentino et al., 2016b; Zuch and Bradham, 2019). We next investigated whether expression of three PMC subset genes, LvJun, LvPks2, and LvVEGFR, is perturbed by VGSC inhibition using smFISH and PMC immunostaining. Jun is a transcription factor that is expressed in the PMC clusters at late gastrula stage (Fig. 6A) (Sun and Ettensohn, 2014). In tricaine-treated embryos, Jun expression is reduced in the VL clusters and expands into the dorsal part of the ring where it is expressed by ectopic PMC clusters (Fig. 6B, G). Notably, the ectopic PMC clusters that arise in tricaine-treated late

gastrula embryos strongly express Jun, while rogue PMCs typically do not. Pks2 is a PMC subset gene which encodes a protein that belongs to the group of polyketide synthases, and it is expressed in PMCs in the ventral and dorsal midline, clusters, and anterior tips of the cords at late gastrula stage (Fig. 6C) (Castoe et al., 2007; Sun and Ettensohn, 2014; Zuch and Bradham, 2019). In tricaine-treated embryos, Pks2 is expressed in the same PMC subsets as controls while also expanding into all of the PMCs in the ventral part of the PMC ring as well as the rogue PMCs (Fig. 6D). In addition, most PMCs in tricaine-treated embryos exhibit highly elevated levels of LvPks2 expression relative to controls (Fig. 6H). LvVEGFR expression is present throughout the entire PMC complement at late gastrula stage and is elevated in the cluster PMCs adjacent to the ectodermal sites of VEGF expression (Fig. 6E) (Duloquin et al., 2007; Adomako-Ankomah and Ettensohn, 2013; Sun and Ettensohn, 2014; Schatzberg et al., 2015; Piacentino et al., 2016a; Piacentino et al., 2016b). In tricaine-

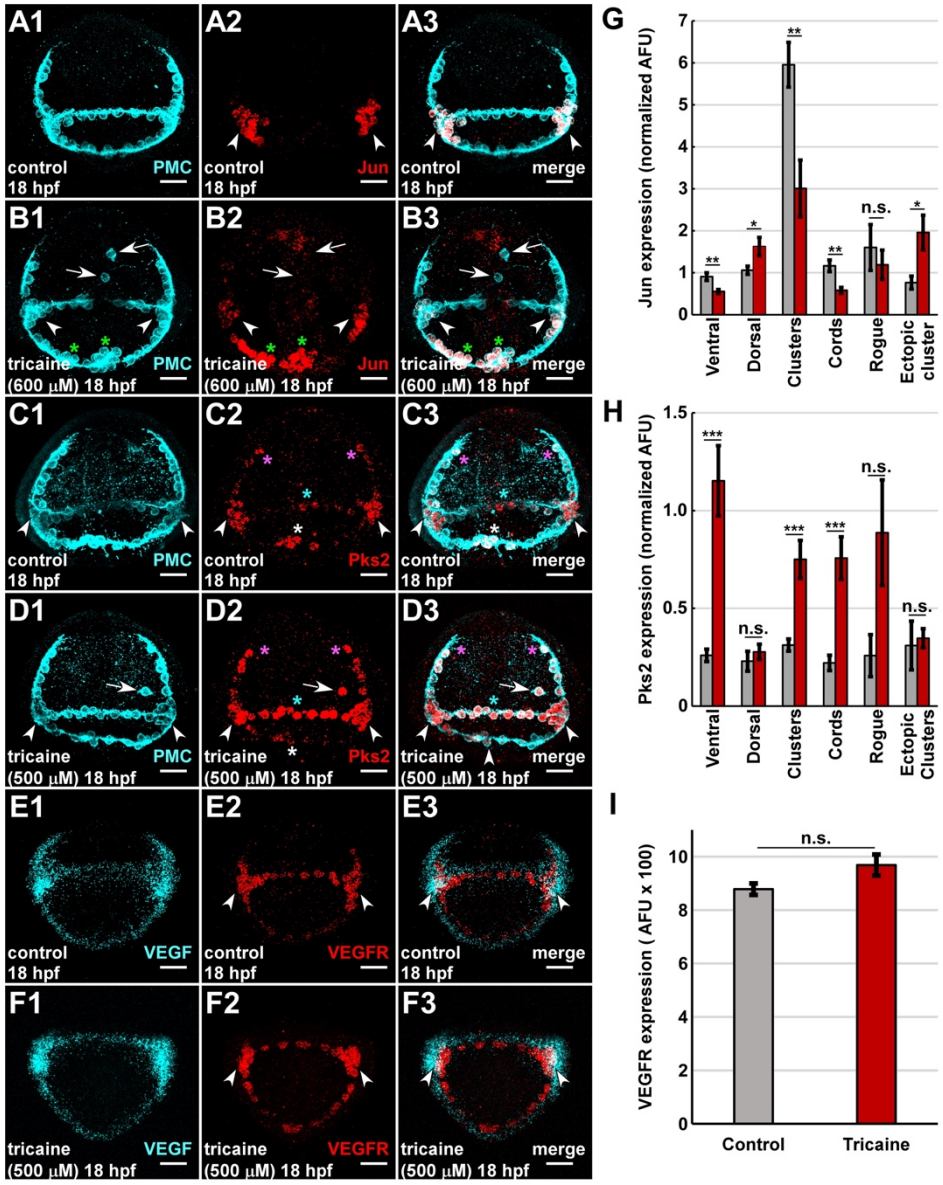

Figure 6. VGSC activity is required for normal spatial expression of PMC subset genes Jun and Pks2 at late gastrula stage.
A-F. Control (A, C, E) and tricaine-treated (B, D, F) late gastrula-stage (18 hpf) embryos were subjected to HCR FISH for Jun, pks2, or VEGFR (red, 2) and PMC immunolabeling (cyan, A1, B1, C1, D1) or FISH for VEGF (cyan, E1, F1), and are shown as confocal z-projections. PMC clusters (white arrowheads), rogue PMCs (arrows), the dorsal midline/scheitel (white asterisks), the ventral midline (cyan asterisks), the cord tips (pink asterisks), and ectopic clusters (green asterisks) are indicated. G-I. The expression levels are shown for each gene as the normalized average signal ± s.e.m. within the indicated PMC territories in addition to rogue PMCs; n ≥ 15 (Jun); n ≥ 15 (Pks2); n ≥ 17 (VEGFR); * $p < 0.05$; ** $p < 10^{-2}$; *** p value $< 10^{-3}$; n.s. not significant (student *t*-test). The scale bars represent 20 µm.

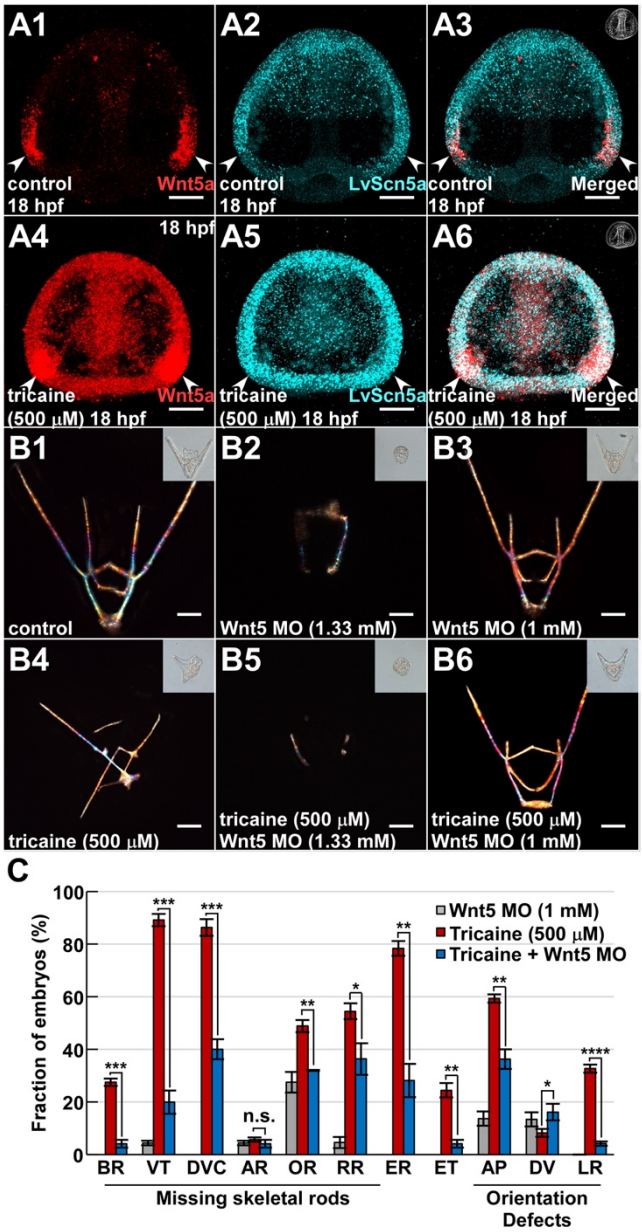

Figure 7. Suboptimal Wnt5 knockdown is sufficient to rescue the tricaine phenotype.
A. Control (A1-3) and tricaine-treated (A4-6) embryos subjected to HCR FISH at late gastrula stage for Wnt5 (red) and LvScn5a (cyan) are shown as confocal z projections. The spatial overlap of expression of these genes in the posterior VL ectoderm is indicated (arrowheads). B. Control embryos (B1, B4) and embryos microinjected with Wnt5 MO at a high dose (B2, 5) or low dose (B3, 6) are shown at the pluteus stage without (B1-3) or with tricaine treatment (B4-6) as skeletal birefringence images with corresponding DIC images inset. C. The frequency of skeletal patterning defects per embryo is shown as the average percentage ± s.e.m.; n ≥ 22 per condition; * $p < 0.05$; ** $p < 10^{-4}$; *** $p < 10^{-8}$; **** $p < 10^{-12}$; ***** $p < 10^{-16}$; n.s. not significant (weighted *t*-test). The scale bars in A represent 20 μm; the remainder are 50 μm.

treated embryos, the ventrolateral VEGFR expression level is not significantly perturbed relative to controls (Fig. 6F, arrowheads, 6I). Taken together, these data show that VGSC inhibition is sufficient to perturb PMC subpopulation identity as reflected by the abnormal spatial expression profiles for Jun and Pks2 in tricaine-treated embryos. Since Jun and Pks2 both exhibit spatially expanded expression, the results suggest that VGSC activity normally functions to restrict Jun and Pks2 expression spatially and to reduce Pks2 expression levels.

Wnt5 reduction is sufficient to rescue tricaine-mediated skeletal patterning defects

Since both Wnt5 and Scn5a are expressed by the posterior VL ectoderm, we next confirmed their spatial overlap using smFISH. smFISH for LvScn5a exhibits greater sensitivity than standard FISH, revealing a general background of expression in many cells, particularly in the anterior half of the embryo, along with higher levels of Scn5a expression in the ventrolateral and apical domains of the ectoderm at 18 hpf (Fig. 7A2). These experiments confirm that tricaine treatment results in a dramatic expansion of the Wnt5 spatial expression domain at late gastrula stage, and that Wnt5 and Scn5a expression spatially overlap in both controls and in tricaine-treated embryos in the posterior ventrolateral ectoderm

(Fig. 7A, arrowheads). Tricaine treatment also resulted in generally elevated Scn5a gene expression (Fig. 7A5). We next asked whether the skeletal patterning defects associated with VGSC inhibition could be rescued by Wnt5 suppression. To test this, zygotes were microinjected with LvWnt5 MO and treated with tricaine, then assessed for skeletal patterning defects at the pluteus stage. Injection of Wnt5 MO at a high dose resulted in inhibition of skeletogenesis, with arrested development at late gastrula stage, consistent with previous findings (McIntyre et al., 2013) (Fig. 7B2, B5). Because our goal was to evaluate skeletal patterning, we performed a dose-response of Wnt5 MO and selected a suboptimal dose that permitted skeletogenesis to occur and for development to proceed beyond late gastrula stage. The majority of embryos injected with a suboptimal dose of Wnt5 MO developed control-like skeletons (Fig. 7B3, C). When Wnt5 MO injection was combined with tricaine treatment, skeletal patterning defects were significantly rescued (Fig. 7B6, C). These results indicate that Wnt5 suppression is sufficient to significantly rescue the skeletal patterning defects induced by VGSC inhibition. These findings suggest that the major skeletal patterning defects associated with tricaine treatment can be explained by

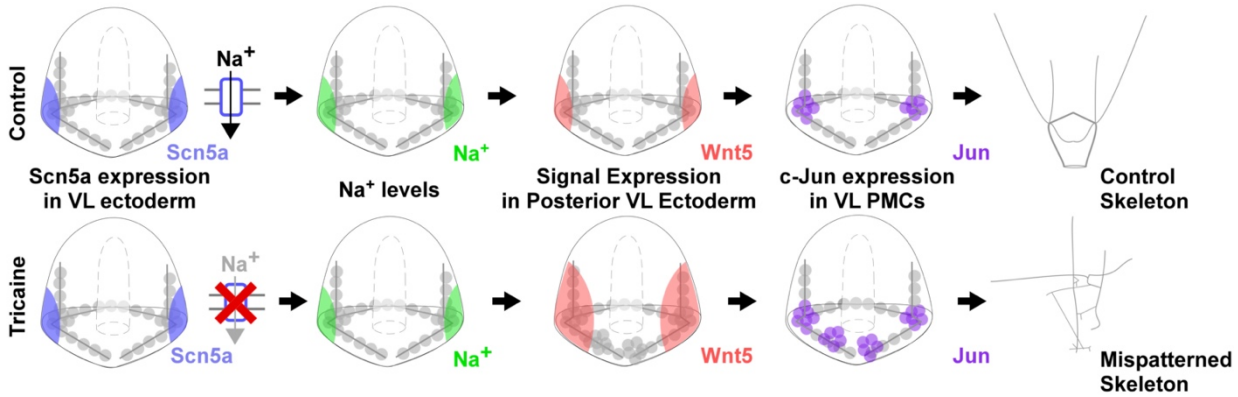

Figure 8. A model for tricaine-mediated skeletal patterning defects.
In controls (upper panel), Scn5a expressed in the posterior VL ectoderm is required for spatially restricted Wnt5 expression in the same ectodermal regions. Bilateral Jun-expressing PMC clusters normally arise adjacent to the VL ectoderm, in which triradiates arise; normally patterned skeletons then develop. VGSC inhibition (lower panel) results in normal sodium ion levels, spatially expanded Wnt5 expression, ectopic Jun-expressing PMC clusters, and abnormal skeletal patterns.

the increase in the spatial expression domain of Wnt5, including AP orientation defects.

Model

These results are consistent with a model in which VGSC activity in the ventrolateral ectoderm functions to spatially restrain Wnt5 expression and signaling. In the absence of VGSC activity, ventrolateral sodium ion levels are unperturbed; however, Wnt5 expression becomes spatially expanded in the posterior ventrolateral ectoderm, ectopic Jun-expressing PMC clusters and triradiates arise, and abnormal skeletal patterning ensues (Fig. 8).

Discussion

Overall, our study presents the novel finding that the activity of LvScn5a, a voltage-gated sodium channel (VGSC), is a previously unrecognized, required regulator of skeletal patterning that functions to restrain the spatial expression of patterning cues VEGF and Wnt5. In this study, we used the local anesthetic tricaine to show that VGSC activity is required for normal skeletal patterning in Lv sea urchin embryos. Inhibition of VGSC activity is sufficient to induce ectopic PMC clusters and triradiates along with skeletal patterning defects. Lv embryos express an endogenous VGSC gene, LvScn5a, in posterior ventrolateral (VL) ectodermal regions that are adjacent to the PMC clusters where skeletogenesis initiates. We show that tricaine-mediated skeletal patterning defects can be rescued by overexpression of an anesthetic insensitive version of LvScn5a, indicating the specificity of tricaine. Finally, we show that the tricaine-mediated skeletal patterning defects are rescued by reduction of Wnt5 expression, demonstrating that the expanded expression of Wnt5 is the functionally relevant effect of VGSC inhibition.

We show that acute tricaine treatment results in depressed sodium ion levels and hyperpolarization, as expected. However, longer-term tricaine treatment results in both depolarization and a return of sodium ions to levels that are comparable to controls. We therefore interpret the depolarization of long-term tricaine-treated embryos to be a result of compensatory mechanisms, likely via other ion channels that restore normal sodium ion levels at the expense of V_{mem}. Similar compensatory changes have been observed after prolonged inhibition (hours) of other ion channels (Schatzberg et al., 2015). Interestingly, tricaine-treated embryos appear to upregulate LvScn5a expression in response to tricaine treatment, which may also indicate an additional compensatory response.

VGSC inhibition results in the formation of ectopic PMC clusters and supernumerary skeletal triradiates. It is well established that ectodermal cues provide spatial information that directs PMC migration (von Ubisch, 1937; Hardin et al., 1992; Armstrong et al., 1993; Duloquin et al., 2007; Adomako-Ankomah and Ettensohn, 2013; McIntyre et al., 2013; Piacentino et al., 2015; Piacentino et al., 2016a; Piacentino et al., 2016b). To date, VEGF is the only signal that is known to be required for PMC cluster formation (Duloquin et al., 2007; Adomako-Ankomah and Ettensohn, 2013).

Our results indicate that Wnt5 signaling is also important for PMC cluster formation. We find that Wnt5 expression in the posterior VL ectoderm is dramatically spatially expanded in response to VGSC inhibition. That expansion correlates with the formation of ectopic PMC clusters and triradiates as well as the production of ectopic skeletal elements, and importantly, is rescued by partial Wnt5 knockdown. That rescue suggests that Wnt5 expression in the VL ectoderm regulates PMC cluster formation and triradiate secretion, and thus identifies Wnt5 as a second cue, along with VEGF, that organizes PMC clusters. Previous work suggested that Wnt5 is a driver of VEGF expression in the posterior VL ectoderm (McIntyre et al., 2013). While we observe a mild spatial expansion of VEGF expression in tricaine-treated embryos, that expansion does not match the dramatic expansion of Wnt5 expression, implying that Wnt5 signaling is a not sufficient to drive VEGF expression, and that the expression of these genes is at least partially independently regulated. Precisely defining that relationship will require further studies.

It could be argued that the ectopic PMC aggregates observed in tricaine-treated embryos do not necessarily have PMC cluster identity and that instead, VGSC inhibition

modulates cell adhesion, thereby producing these extra PMC aggregates. However, previous work has shown that c-Jun is a PMC subset gene whose expression marks the PMC clusters at late gastrula stage (Sun and Ettensohn, 2014); therefore, the expression of c-Jun in these PMC aggregates suggests that they are, indeed, ectopically positioned PMC clusters. Moreover, the occurrence of ectopic, supernumerary triradiates in VGSC-inhibited embryos reinforces the conclusion that the ectopic PMC aggregates therein indeed have PMC cluster identity. Our data are thus consistent with a model in which Wnt5 signaling from the posterior VL ectoderm is sufficient to organize ectopic clusters of PMCs that express c-Jun and produce triradiates or other skeletal rods. This would suggest a novel and as of yet unreported role for Wnt5 in sea urchin embryonic development and prompts further inquiry into the relationship between Wnt5 signaling and PMC subset gene expression.

It remains unclear how VGSC inhibition modulates Wnt5 expression levels. Tricaine treatment abolishes the regenerative response of the tail in *Xenopus*; this effect is due to changes in intracellular sodium ion levels and not V_{mem}, and is mediated by the salt inducible kinase (SIK) (Sanz, 2003; Tseng et al., 2010). Thus, SIK is an intriguing prospect as a mediator of the Scn5a activity in sea urchins. However, the Lv SIK ortholog is expressed at relatively low levels during skeletal patterning (Hogan et al., 2020). Further, in tricaine-treated embryos, we observe normal sodium ion levels during the temporal window of VGSC functional relevance along with abnormal V_{mem}, which is inconsistent with effects mediated by perturbation to sodium ion levels or to SIK.

Alternatively, the overlapping ectodermal expression domains of Wnt5 and LvScn5a are consistent with the possibility that Scn5a activity negatively regulates Wnt5 spatial expression by interrupting a “community effect” by which Wnt5 expression spreads among cells via Wnt5 signaling-dependent transcription that activates Wnt5 expression. Such community effects are known to regulate the expression of Wnt8 via β-catenin/TCF (Minokawa et al., 2005). While it is currently unknown whether Wnt5 similarly signals via β-catenin, Wnt5 signaling is sufficient to mediate gene expression changes (McIntyre et al., 2013), implying that a community effect could occur whether it relies on β-catenin/TCF or on a different transcription factor. It is generally unknown how boundaries are established that halt community effects; our results are consistent with a model in which V_{mem} status negatively regulates this community effect. Specifically, it suggests that a mildly depolarized state is inhibitory, whereas the strongly depolarized state that results from VGSC inhibition is not, allowing the Wnt5 expression domain to be abnormally large. If correct, this model would intriguingly tie biophysical states to gene expression control. In a correlate model, the extent of Wnt5 extracellular diffusion or transport could be modulated by the degree of depolarization to achieve a similar result by impinging on the community effect at the level of the signal.

An alternative possibility is that VGSC activity influences the expression of a microRNA (miRNA), in keeping with the role that miR-31 exerts to spatially modulate the expression of Wnt1 and Eve expression within the posterior ectoderm (Sampilo et al., 2021). Perhaps another miRNA similarly regulates Wnt5 expression to constrain it spatially, and is in turn regulated by VGSC activity. However, while miRNAs have been shown to regulate ion channel expression (Gross et al., 2016; Liu et al., 2016; Shao et al., 2016; Sakai et al., 2017; Gross and Tiwari, 2018), evidence for the converse regulation is currently more sparse. One study demonstrates that the anion channel, CFTR, regulates

miRNA expression in mammalian embryos via bicarbonate influx and subsequent downstream signaling events (Lu et al., 2012), while another study shows that epithelial sodium channels negatively regulate the expression of two miRNAs in mammalian embryos (Sun et al., 2014). Potential VGSC-mediated impacts on miRNA expression or on a Wnt5 community effect are not mutually exclusive: both might contribute to regulating the spatial extent of Wnt5 expression. A molecular understanding of how VGSC activity controls the spatial expression of Wnt5 will be an important next step in unraveling the mechanisms that regulate sea urchin skeletal patterning.

Methods

Reagents

Chemicals were obtained from Sigma Aldrich or Fisher Scientific. Ethyl 3-amino-benzoate methanesulfonate (tricaine) was obtained from Sigma Aldrich (St. Louis, MO), Bis-(1,3-diethylthiobarbituric acid)trimethine oxonol (DiSBAC, relative polarization) and CoroNa green, acetoxymethyl ester (CoroNa, sodium ions) were purchased from Invitrogen (Waltham, MA) .

Embryo culture, microinjection, drug treatment, and imaging

Lytechinus variegatus adults were obtained from either Reeftopia (Miami, FL) or the Duke University Marine Labs (Beaufort, NC). Gamete harvesting, embryo culturing, in vitro transcription, and microinjections were performed as previously described (Bradham and McClay, 2006; Piacentino et al., 2015). The Wnt5 MO was obtained from GeneTools. The Wnt-5 MO sequence is: (5′-CGCTGGCAGACAAAGGGCGACTCGA-3′) (McIntyre et al., 2013). Tricaine methanesulfonate (Sigma) was resuspended in artificial sea water (ASW) and was stored at −20°C in single use aliquots. Tricaine treatments were performed using artificial sea water that was buffered to pH 8.1 using NaHCO3. Dose-response experiments were performed with all reagents to determine their optimal working concentrations. Embryos were imaged on a Zeiss Axioplan microscope at 200X with differential interference contrast (DIC) for morphology or with plane-polarized light to capture skeletal birefringence as a series of images in multiple focal planes. Montages of the focal planes were manually assembled using CanvasX (Canvas GFX, inc, Boston, MA) to present the entire skeleton in focus. All focal planes were used for scoring with our in-house scoring rubric (Piacentino et al., 2016), which encompasses element shortening, lengthening, loss, duplication, or transformation, ectopic element production, abnormal element orientation, as well as whole embryo-level defects such as midline defects.

LvScn5a DR construct

A sequence encoding the drug-resistant (DR) F1715A mutation was cloned into the pCS2 vector for in vitro transcription (Genscript, Inc. Piscataway, NJ).

Fluorescent in situ hybridization (FISH)

Antisense riboprobes for LvVEGF, LvVEGFR, LvWnt5, LvUnivin, LvChordin, and LvIrxA were previously described (Bradham et al., 2009; McIntyre et al., 2013; Piacentino et al., 2015; Schatzberg et al., 2021). In situ hybridization was performed as previously described using digoxigenin-labeled probes (Piacentino et al., 2015).

HCR FISH, Immunolabeling, and confocal microscopy

Probe sets were designed from the open reading frames by Molecular Instruments, Inc. (Los Angeles, CA, USA). Embryos were fixed in 4% paraformaldehyde then subjected to hybridization chain-reaction (HCR) single molecule FISH (Choi et al., 2016; Choi et al., 2018) using fluorescently labeled amplifiers, buffers, and probe sets from Molecular Instruments, Inc. per the manufacturer's instructions. Embryos were incubated in hairpin solution overnight in the dark at room temperature, washed with 5X SSCT, then mounted

in PBS with 50% glycerol for imaging. Immunofluorescent labeling was performed as previously described (Bradham et al., 2009). Primary antibodies were neural-specific monoclonal 1e11 (1:10, a gift from Robert Burke, University of Victoria, BC, Canada), anti-serotonin polyclonal (1:1000, Sigma-Aldrich), ciliary band-specific monoclonal 295 (undiluted; a gift from David McClay, Duke University, Durham, NC), and PMC-specific monoclonal 6a9 (1:5; a gift from Charles Ettensohn, Carnegie Mellon University, Pittsburgh, PA). Fluorescent secondary antibodies Cy2-conjugated goat anti-rabbit (1:900) and Cy3-conjugated goat anti-mouse (1:300) were obtained from Jackson Labs (West Grove, PA). Confocal imaging was performed using an Olympus FV10i laser-scanning confocal microscope. Confocal z-stacks were maximally projected using Fiji, and maximum intensity z-projections are presented.

Spatial gene expression analysis

For LvWnt5, LvVEGF, and LvUnivin FISH results, a threshold was applied to z-projected embryos in Fiji to produce binary images. ROIs were then defined in an automated manner using the Analyze Particles function in Fiji after adjusting the parameters of the threshold to most accurately capture the expression. The resulting area values were then normalized to the total area of the z-projected embryo. For LvChd and LvIrxA, embryos were imaged in vegetal views using an FV10i laser-scanning confocal microscope to allow for clear discrimination between ventral and dorsal territories. Confocal z-stack projections were analyzed in CanvasX (Canvas GFX, Inc., Boston, MA). Using the gut as the origin, the angles of the LvIrxA and LvChd expression domains were measured. The size of the inferred ciliary band was determined per embryo by subtracting the sum of the Chd and IrxA angles from 360°.

PMC subset gene expression analysis

For LvJun and LvPks2 smFISH results, ROIs were manually drawn around each PMC using Fiji, and the mean fluorescence intensity of the Jun or Pks2 signal was measured and normalized to z-depth by dividing by either the hoechst (nuclei) or PMC stain fluorescence intensity for the respective PMC. Each image was background corrected by sampling empty space at the corners of the images then subtracting the average background per area from other signal intensities. Identical acquisition settings were used across all embryos within each experiment to ensure their comparability.

Fluorescent ion reporters, acute tricaine treatment, and quantitations

CoroNa and DiSBAC were used as previously described (Rodriguez-Sastre et al., 2019) and embryos were imaged live on an Olympus FV10i laser scanning confocal microscope. Embryos acutely treated with tricaine were cultured in ASW without inhibitor until time of imaging; they were then placed in a tricaine bath and imaged within 10 minutes. Raw 16-bit images of single z-slices were quantitated using Fiji by placing ROIs in distinct locations throughout the embryo in a stereotypic manner across all embryos. The mean fluorescence value per area was then measured from each ROI, and each image was background corrected as described above. Identical acquisition settings were used across all embryos within each experiment to ensure their comparability.

Author Contributions

This study was conceived by CAB and designed by CAB and CFT. The experiments were executed by CFT, VS, SM, ZY, and JG; data analyses were performed by CFT, DYH, VS, SM, ZY, and JG; The manuscript was written by CFT and CAB, and edited by all co-authors.

Acknowledgments

We thank Professors Charles Ettensohn, Robert Burke, and David McClay for their gifts of antibodies, and Dr. Todd Blute for microscopy advice. This work was supported by NSF IOS 1656752 (CAB). VS was partially supported by the BU Biology Undergraduate Research Opportunities Program (UROP). SM and JG were partially supported by the BU Biology Summer Undergraduate Research Fellowship (SURF) program.

Competing Interests

The authors declare no competing or financial interests.

References

Adams, D.S., Levin, M., 2012. Measuring resting membrane potential using the fluorescent voltage reporters DiBAC4(3) and CC2-DMPE. Cold Spring Harbor protocols 2012, 459-464.

Adams, D.S., Masi, A., Levin, M., 2007. H+ pump-dependent changes in membrane voltage are an early mechanism necessary and sufficient to induce Xenopus tail regeneration. Development (Cambridge, England) 134, 1323-1335.

Adams, D.S., Robinson, K.R., Fukumoto, T., Yuan, S., Albertson, R.C., Yelick, P., Kuo, L., McSweeney, M., Levin, M., 2006. Early, H+-V-ATPase-dependent proton flux is necessary for consistent left-right patterning of non-mammalian vertebrates. Development (Cambridge, England) 133, 1657-1671.

Adomako-Ankomah, A., Ettensohn, C.A., 2013. Growth factor-mediated mesodermal cell guidance and skeletogenesis during sea urchin gastrulation. Development (Cambridge, England) 140, 4214-4225.

Akasaka, K., Uemoto, H., Wilt, F., Mitsunaga-Nakatsubo, K., Shimada, H., 1997. Oral-aboral ectoderm differentiation of sea urchin embryos is disrupted in response to calcium ionophore. Development, growth & differentiation 39, 373-379.

Armstrong, N., Hardin, J., McClay, D.R., 1993. Cell-cell interactions regulate skeleton formation in the sea urchin embryo. Development (Cambridge, England) 119, 833-840.

Attili, S., Hughes, S.M., 2014. Anaesthetic tricaine acts preferentially on neural voltage-gated sodium channels and fails to block directly evoked muscle contraction. PloS one 9, e103751.

Beane, W.S., Morokuma, J., Lemire, J.M., Levin, M., 2013. Bioelectric signaling regulates head and organ size during planarian regeneration. Development (Cambridge, England) 140, 313-322.

Bergeron, K.-F., Xu, X., Brandhorst, B.P., 2011. Oral–aboral patterning and gastrulation of sea urchin embryos depend on sulfated glycosaminoglycans. Mechanisms of development 128, 71-89.

Brackenbury, W.J., Djamgoz, M.B., Isom, L.L., 2008. An emerging role for voltage-gated Na+ channels in cellular migration: regulation of central nervous system development and potentiation of invasive cancers. The Neuroscientist 14, 571-583.

Bradham, C.A., Oikonomou, C., Kühn, A., Core, A.B., Modell, J.W., McClay, D.R., Poustka, A.J., 2009. Chordin is required for neural but not axial development in sea urchin embryos. Developmental biology 328, 221-233.

Cakir, Y., Strauch, S.M., 2005. Tricaine (MS-222) is a safe anesthetic compound compared to benzocaine and pentobarbital to induce anesthesia in leopard frogs (Rana pipiens). Pharmacological reports : PR 57, 467-474.

Carboni, M., Zhang, Z.-S., Nepliouevа, V., Starmer, C., Grant, A., 2005. Slow sodium channel inactivation and use-dependent block modulated by the same domain IV S6 residue. The Journal of membrane biology 207, 107-117.

Castoe, T.A., Stephens, T., Noonan, B.P., Calestani, C., 2007. A novel group of type I polyketide synthases (PKS) in animals and the complex phylogenomics of PKSs. Gene 392, 47-58.

Catterall, W.A., 2000. From ionic currents to molecular mechanisms: the structure and function of voltage-gated sodium channels. Neuron 26, 13-25.

Catterall, W.A., 2014. Structure and function of voltage‐gated sodium channels at atomic resolution. Experimental physiology 99, 35-51.

Chopra, S.S., Stroud, D.M., Watanabe, H., Bennett, J.S., Burns, C.G., Wells, K.S., Yang, T., Zhong, T.P., Roden, D.M., 2010. Voltage-gated sodium channels are required for heart development in zebrafish. Circulation research 106, 1342-1350.

Cole, R.W., Woodruff, R.I., 2000. Vitellogenic ovarian follicles of Drosophila exhibit a charge-dependent distribution of endogenous soluble proteins. Journal of insect physiology 46, 1239-1248.

Croce, J., Lhomond, G., Gache, C., 2003. Coquillette, a sea urchin T-box gene of the Tbx2 subfamily, is expressed asymmetrically along the oral–aboral axis of the embryo and is involved in skeletogenesis. Mechanisms of development 120, 561-572.

Duboc, V., Rottinger, E., Besnardeau, L., Lepage, T., 2004. Nodal and BMP2/4 signaling organizes the oral-aboral axis of the sea urchin embryo. Developmental cell 6, 397-410.

Duloquin, L., Lhomond, G., Gache, C., 2007. Localized VEGF signaling from ectoderm to mesenchyme cells controls morphogenesis of the sea urchin embryo skeleton. Development (Cambridge, England) 134, 2293-2302.

Epps, D.E., Wolfe, M.L., Groppi, V., 1994. Characterization of the steady-state and dynamic fluorescence properties of the potential-sensitive dye bis-(1,3-dibutylbarbituric acid)trimethine oxonol (Dibac4(3)) in model systems and cells. Chemistry and physics of lipids 69, 137-150.

Ettensohn, C.A., Malinda, K.M., 1993. Size regulation and morphogenesis: a cellular analysis of skeletogenesis in the sea urchin embryo. Development (Cambridge, England) 119, 155-167.

Frazier, D.T., Narahashi, T., 1975. Tricaine (MS-222): effects on ionic conductances of squid axon membranes. European journal of pharmacology 33, 313-317.

Gross, C., Tiwari, D., 2018. Regulation of ion channels by microRNAs and the implication for epilepsy. Current neurology and neuroscience reports 18, 1-11.

Gross, C., Yao, X., Engel, T., Tiwari, D., Xing, L., Rowley, S., Danielson, S.W., Thomas, K.T., Jimenez-Mateos, E.M., Schroeder, L.M., 2016. MicroRNA-mediated downregulation of the potassium channel Kv4. 2 contributes to seizure onset. Cell reports 17, 37-45.

Gross, J.M., Peterson, R.E., Wu, S.-Y., McClay, D.R., 2003. LvTbx2/3: a T-box family transcription factor involved in formation of the oral/aboral axis of the sea urchin embryo.

Hardin, J., Coffman, J.A., Black, S.D., McCLAY, D.R., 1992. Commitment along the dorsoventral axis of the sea urchin embryo is altered in response to NiCl2. Development (Cambridge, England) 116, 671-685.

Harris, J.B., Pollard, S.L., 1986. Neuromuscular transmission in the murine mutants "motor end-plate disease" and "jolting". Journal of the neurological sciences 76, 239-253.

Hibino, T., Ishii, Y., Levin, M., Nishino, A., 2006. Ion flow regulates left-right asymmetry in sea urchin development. Development genes and evolution 216, 265-276.

Hogan, J.D., Keenan, J.L., Luo, L., Ibn-Salem, J., Lamba, A., Schatzberg, D., Piacentino, M.L., Zuch, D.T., Core, A.B., Blumberg, C., 2020. The developmental transcriptome for Lytechinus variegatus exhibits temporally punctuated gene expression changes. Developmental biology 460, 139-154.

Hu, M.Y., Yan, J.J., Petersen, I., Himmerkus, N., Bleich, M., Stumpp, M., 2018. A SLC4 family bicarbonate transporter is critical for intracellular pH regulation and biomineralization in sea urchin embryos. eLife 7.

Jaffe, L.A., 1976. Fast block to polyspermy in sea urchin eggs is electrically mediated. Nature 261, 68-71.

Kawakami, Y., Raya, A., Raya, R.M., Rodriguez-Esteban, C., Izpisua Belmonte, J.C., 2005. Retinoic acid signalling links left-right asymmetric patterning and bilaterally symmetric somitogenesis in the zebrafish embryo. Nature 435, 165-171.

Letcher, J., 1992. Intracelomic use of tricaine methanesulfonate for anesthesia of bullfrogs (Rana catesbeiana) and leopard frogs (Rana pipiens). Zoo biology 11, 243-251.

Levin, M., 2012. Molecular bioelectricity in developmental biology: new tools and recent discoveries: control of cell behavior and pattern formation by transmembrane potential gradients. BioEssays : news and reviews in molecular, cellular and developmental biology 34, 205-217.

Levin, M., 2014. Molecular bioelectricity: how endogenous voltage potentials control cell behavior and instruct pattern regulation in vivo. Molecular biology of the cell 25, 3835-3850.

Liu, X., Zhang, Y., Du, W., Liang, H., He, H., Zhang, L., Pan, Z., Li, X., Xu, C., Zhou, Y., 2016. MiR-223-3p as a novel MicroRNA regulator of expression of voltage-gated K+ channel Kv4. 2 in acute myocardial infarction. Cellular Physiology and Biochemistry 39, 102-114.

Lu, Y.C., Chen, H., Fok, K.L., Tsang, L.L., Yu, M.K., Zhang, X.H., Chen, J., Jiang, X., Chung, Y.W., Ma, A.C.H., 2012. CFTR mediates bicarbonate-dependent activation of miR-125b in preimplantation embryo development. Cell research 22, 1453-1466.

Lyons, D.C., Kaltenbach, S.L., McClay, D.R., 2012. Morphogenesis in sea urchin embryos: linking cellular events to gene regulatory network states. Wiley interdisciplinary reviews. Developmental biology 1, 231-252.

McIntyre, D.C., Seay, N.W., Croce, J.C., McClay, D.R., 2013. Short-range Wnt5 signaling initiates specification of sea urchin posterior ectoderm. Development (Cambridge, England) 140, 4881-4889.

Meier, S.D., Kovalchuk, Y., Rose, C.R., 2006. Properties of the new fluorescent Na+ indicator CoroNa Green: comparison with SBFI and confocal Na+ imaging. Journal of neuroscience methods 155, 251-259.

Minokawa, T., Wikramanayake, A.H., Davidson, E.H., 2005. cis-Regulatory inputs of the wnt8 gene in the sea urchin endomesoderm network. Developmental biology 288, 545-558.

Nau, C., Wang, G., 2004. Interactions of local anesthetics with voltage-gated Na+ channels. The Journal of membrane biology 201, 1-8.

Nau, C., Wang, S.-Y., Strichartz, G.R., Wang, G.K., 2000. Block of human heart hH1 sodium channels by the enantiomers of bupivacaine. The Journal of the American Society of Anesthesiologists 93, 1022-1033.

Nuccitelli, R., 2003. Endogenous electric fields in embryos during development, regeneration and wound healing. Radiation protection dosimetry 106, 375-383.

Piacentino, M.L., Chung, O., Ramachandran, J., Zuch, D.T., Yu, J., Conaway, E.A., Reyna, A.E., Bradham, C.A., 2016a. Zygotic LvBMP5-8 is required for skeletal patterning and for left-right but not dorsal-ventral specification in the sea urchin embryo. Dev Biol 412, 44-56.

Piacentino, M.L., Ramachandran, J., Bradham, C.A., 2015. Late Alk4/5/7 signaling is required for anterior skeletal patterning in sea urchin embryos. Development (Cambridge, England) 142, 943-952.

Piacentino, M.L., Zuch, D.T., Fishman, J., Rose, S., Speranza, E.E., Li, C., Yu, J., Chung, O., Ramachandran, J., Ferrell, P., Patel, V., Reyna, A., Hameeduddin, H., Chaves, J., Hewitt, F.B., Bardot, E., Lee, D., Core, A.B., Hogan, J.D., Keenan, J.L., Luo, L., Coulombe-Huntington, J., Blute, T.A., Oleinik, E., Ibn-Salem, J., Poustka, A.J., Bradham, C.A., 2016b. RNA-Seq identifies SPGs as a ventral skeletal patterning cue in sea urchins. Development (Cambridge, England) 143, 703-714.

Planells-Cases, R., Caprini, M., Zhang, J., Rockenstein, E.M., Rivera, R.R., Murre, C., Masliah, E., Montal, M., 2000. Neuronal death and perinatal lethality in voltage-gated sodium channel alpha(II)-deficient mice. Biophysical journal 78, 2878-2891.

Pless, S.A., Galpin, J.D., Frankel, A., Ahern, C.A., 2011. Molecular basis for class Ib anti-arrhythmic inhibition of cardiac sodium channels. Nature communications 2, 1-9.

Ragsdale, D.S., McPhee, J.C., Scheuer, T., Catterall, W.A., 1994. Molecular determinants of state-dependent block of Na+ channels by local anesthetics. Science 265, 1724-1728.

Ramlochansingh, C., Branoner, F., Chagnaud, B.P., Straka, H., 2014. Efficacy of tricaine methanesulfonate (MS-222) as an anesthetic agent for blocking sensory-motor responses in Xenopus laevis tadpoles. PloS one 9, e101606.

Rodriguez-Sastre, N., Thomas, C.F., Bradham, C.A., 2019. Measuring voltage and ion concentrations in live embryos. Methods in cell biology 151, 459-472.

Sakai, A., Saitow, F., Maruyama, M., Miyake, N., Miyake, K., Shimada, T., Okada, T., Suzuki, H., 2017. MicroRNA cluster miR-17-92 regulates multiple functionally related voltage-gated potassium channels in chronic neuropathic pain. Nature communications 8, 1-13.

Sampilo, N.F., Stepicheva, N.A., Song, J.L., 2021. microRNA-31 regulates skeletogenesis by direct suppression of Eve and Wnt1. Developmental biology 472, 98-114.

Sanz, P., 2003. Snf1 protein kinase: a key player in the response to cellular stress in yeast. Biochemical Society Transactions 31, 178-181.

Schatzberg, D., Lawton, M., Hadyniak, S.E., Ross, E.J., Carney, T., Beane, W.S., Levin, M., Bradham, C.A., 2015. H(+)/K(+) ATPase activity is required for biomineralization in sea urchin embryos. Dev Biol 406, 259-270.

Schoettger, R.A., 1967. Annotated bibliography on MS-222. US Fish and Wildlife Service.

Shao, J., Cao, J., Wang, J., Ren, X., Su, S., Li, M., Li, Z., Zhao, Q., Zang, W., 2016. MicroRNA-30b regulates expression of the sodium channel Nav1. 7 in nerve injury-induced neuropathic pain in the rat. Molecular pain 12, 1744806916671523.

Shipp, L.E., Hamdoun, A., 2012. ATP‐binding cassette (ABC) transporter expression and localization in sea urchin development. Developmental Dynamics 241, 1111-1124.

Stoetzer, C., Reuter, S., Doll, T., Foadi, N., Wegner, F., Leffler, A., 2016. Inhibition of the cardiac Na+ channel α-subunit Nav1. 5 by propofol and dexmedetomidine. Naunyn-Schmiedeberg's archives of pharmacology 389, 315-325.

Stumpp, M., Hu, M.Y., Melzner, F., Gutowska, M.A., Dorey, N., Himmerkus, N., Holtmann, W.C., Dupont, S.T., Thorndyke, M.C., Bleich, M., 2012. Acidified seawater impacts sea urchin larvae pH regulatory systems relevant for calcification. Proceedings of the National Academy of Sciences of the United States of America 109, 18192-18197.

Sun, X., Ruan, Y.C., Guo, J., Chen, H., Tsang, L.L., Zhang, X., Jiang, X., Chan, H.C., 2014. Regulation of miR-101/miR-199a-3p by the epithelial sodium channel during embryo implantation: involvement of CREB phosphorylation. Reproduction (Cambridge, England) 148, 559-568.

Sun, Z., Ettensohn, C.A., 2014. Signal-dependent regulation of the sea urchin skeletogenic gene regulatory network. Gene expression patterns : GEP 16, 93-103.

Tseng, A.-S., Beane, W.S., Lemire, J.M., Masi, A., Levin, M., 2010. Induction of vertebrate regeneration by a transient sodium current. Journal of Neuroscience 30, 13192-13200.

Vidavsky, N., Addadi, S., Mahamid, J., Shimoni, E., Ben-Ezra, D., Shpigel, M., Weiner, S., Addadi, L., 2014. Initial stages of calcium uptake and mineral deposition in sea urchin embryos. Proceedings of the National Academy of Sciences of the United States of America 111, 39-44.

von Ubisch, L., 1937. Di Normale Skelettbildung bei Echinocyamus pusillus und Psamechinus miliaris und die Bedeutung dieser Vorgänge für die Analyse der Skelette von Keimblatt-Chimären. Z. wiss. Zool 149, 402-476.

Wright, S.N., Wang, S.-Y., Wang, G.K., 1998. Lysine point mutations in Na+ channel D4-S6 reduce inactivated channel block by local anesthetics. Molecular pharmacology 54, 733-739.

Yaguchi, S., Yaguchi, J., Angerer, R.C., Angerer, L.M., Burke, R.D., 2010. TGFβ signaling positions the ciliary band and patterns neurons in the sea urchin embryo. Developmental biology 347, 71-81.

Yu, F.H., Mantegazza, M., Westenbroek, R.E., Robbins, C.A., Kalume, F., Burton, K.A., Spain, W.J., McKnight, G.S., Scheuer, T., Catterall, W.A., 2006. Reduced sodium current in GABAergic interneurons in a mouse model of severe myoclonic epilepsy in infancy. Nature neuroscience 9, 1142-1149.

Zuch, D.T., Bradham, C.A., 2019. Spatially mapping gene expression in sea urchin primary mesenchyme cells. Methods in cell biology 151, 433-442.